Photodissociation dynamics of vibrationally excited CH_2Cl_2 molecules

Ran Marom, Amir Golan, Salman Rosenwaks [1], Ilana Bar [*,2]

Department of Physics, Ben-Gurion University of the Negev, Beer-Sheva 84105, Israel

Received 17 June 2003; in final form 29 July 2003
Published online: 26 August 2003

Abstract

Photodissociation of dichloromethane excited to the second C–H stretch overtone was performed by $\sim$235 nm photons that also tagged the Cl $^2P_{3/2}$ [Cl] and spin–orbit excited Cl $^2P_{1/2}$ [Cl*] photofragments via resonantly enhanced multiphoton ionization. The measured time-of-flight profiles together with the determined Cl*/Cl branching ratio suggest fast dissociation and involvement of several upper states of different symmetries mixing via curve crossing to release both Cl and Cl*. The determined ratio is higher than that obtained previously in the direct, almost isoenergetic, photodissociation of CH_2Cl_2 implying higher non-adiabaticity for vibrationally excited than for vibrationless ground state molecules.
© 2003 Elsevier B.V. All rights reserved.

1. Introduction

Alkyl halides have become the subject of significant study in recent years due to their atmospheric relevance and interesting photodissociation dynamics. Numerous theoretical and experimental investigations on monohalogen alkyl molecules [1–17] have revealed the importance of non-adiabatic curve crossing dynamics in C–X (X = Cl, Br, and I) bond rupture and in generation of ground state $X(^2P_{3/2})$ [X] and spin–orbit excited $X(^2P_{1/2})$ [X*]. Fewer studies have been performed on dihalide alkyl molecules [7,17–20], since the presence of two C–X bonds makes the structure of the electronically excited states and therefore of the UV absorption spectra more complex. Besides, the picture is further complicated by the greater number of potential dissociation pathways.

An important aspect regarding these studies is the impact of initial state preparation on the yield of the ground and spin–orbit excited halogen atoms. For instance, it was shown that in CH_3I dissociation the I*/I product branching measures the behavior of the molecule through the conical intersection of the $^1Q_1$ and $^3Q_0$ potential energy surfaces [4,5,9,10]. Particularly, the non-adiabatic transitions from $^3Q_0$ to $^1Q_1$ were enhanced by

excitation of parent bending [4,5], or methyl rocking [3] due to the destruction of the C_{3v} symmetry. An increase in the branching ratio into Cl* was also observed by Lambert and Dagdigian [15,16] in vibrationally mediated photodissociation (VMP) [21,22] of CH_3Cl and CHD_2Cl pre-excited to the fourth overtone of the C–H stretch, with a larger increase in the former. Furthermore, we encountered alteration of the branching ratio in the VMP of CH_3CF_2Cl and CH_3CFCl_2, as compared to the almost isoenergetic vibrationless ground state photodissociation [23–25]. However, this is not always the case as revealed by VMP of CHF_2Cl, which did not affect the Cl*/Cl branching ratio probably due to a smaller variation in the photolysis dynamics relative to that of vibrationless ground state molecules [26].

In the present study, the dissociation of dichloromethane, CH_2Cl_2, pre-excited to the region of the second C–H stretch overtone is explored. The room temperature photoacoustic (PA) vibrational spectrum and the jet-cooled Cl and Cl* action spectra show that the vibrational energy structure is quite complex due to strong Fermi resonances between stretching and HCH bending vibrations, providing some insight on the intramolecular dynamics. The measured Cl*/Cl branching ratios together with the translational energy distributions and anisotropy parameters, β, obtained from measured time-of-arrival profiles of ^{35}Cl and $^{35}Cl*$ characterize the primary decay process and allow to examine the effect of the vibrational motion on the branching.

2. Experiment

The experiments were performed with the previously described setup [22–28]. The photodissociation was carried out in a home-built time-of-flight mass spectrometer (TOFMS) providing sensitive and mass-selective detection. The CH_2Cl_2 sample (99.9+% purity) was thoroughly degassed at reduced temperatures and its gas phase was mixed with Ar to provide a ~10% mixture at a total pressure of ~760 Torr. The molecular beam was expanded into the ionization chamber perpendicularly to the TOFMS axis and the laser

beams (see below). The expansion was carried out through a nozzle-skimmer arrangement, to typical pressures of $\sim 5 \times 10^{-6}$ Torr. Under these conditions the beam was characterized by a predominant rotational temperature of ~10 K and vibrational temperature of <100 K. The molecular beam was intersected by a near infrared (NIR) laser beam around 1151 nm, from the idler of an optical parametric oscillator ($E \sim 12$ mJ, bandwidth ~0.08 cm^{-1}), which vibrationally excited the parent molecule in the region of three C–H stretch quanta. Following the excitation pulse, after a delay of ~10 ns, the excited CH_2Cl_2 molecules were photodissociated by a counterpropagating UV beam (~130 μJ) from a frequency doubled tunable dye laser (~0.4 cm^{-1}). The wavelength of this beam was chosen to match the two-photon transition of Cl (4p $^2D_{3/2} \leftarrow$ 3p $^2P_{3/2}$) at 235.336 nm and Cl* (4p $^2P_{1/2} \leftarrow$ 3p $^2P_{1/2}$) at 235.205 nm to also interrogate the Cl and Cl* photofragments, respectively, by (2 + 1) resonantly enhanced multiphoton ionization (REMPI). The NIR beam was focused with a 15 cm focal length (f.l.) lens, while the photolysis/probe (UV) beam with a 30 cm f.l. lens. The CH_2Cl_2 molecules were photolyzed efficiently only when overtone excitation was induced, due to the very low absorption cross section of vibrationless ground state molecules at ~235 nm (1.16×10^{-22} cm^2) [29].

Ions formed via REMPI in the focal volume were subject to continuously biased extraction, two acceleration stages, two pairs of orthogonal deflection plates and an einzel lens. The ions then entered the field-free drift region (55 cm long) and were eventually detected by a microsphere plate (MSP). The MSP output was amplified and fed into a digital oscilloscope and a boxcar integrator where wavelength-dependent ion signals of ^{35}Cl, ^{37}Cl, $^{35}Cl*$, and $^{37}Cl*$ were captured and processed by a computer. The signals of masses 35 and 37 were monitored simultaneously by two independent boxcar channels, taking advantage of the mass resolution of the TOFMS. Action spectra measuring the yield of the released Cl and Cl* photofragments as a function of the NIR wavelength laser were monitored by setting the UV laser on the corresponding chlorine transitions. Each data point in the ensuing spectra was an

average of thirty pulses. In addition, Doppler profiles were measured to determine the Cl*/Cl branching ratios, by fixing the NIR laser on the Q-branch of the most intense band (see below) and scanning the UV laser across the Cl and Cl* transitions. The profiles were well fitted by Gaussians and their areas were used to extract the Cl*/Cl branching ratio once the scaling factor of the above-mentioned transitions was accounted for [30]. Furthermore, time-of-arrival profiles of the ^{35}Cl and ^{35}Cl* resulting from 5000 shots were recorded, setting the NIR laser on the Q-branch transition and the UV laser on the Cl and Cl* transitions, with the digital oscilloscope and stored for later analysis. The time-of-arrival profiles were measured under space focusing conditions at two different geometries, vertical (UV laser polarization perpendicular to the TOF axis) and horizontal (UV laser polarization parallel to the TOF axis). The effects of the apparatus on the TOF were previously determined [27,28], allowing calibration of the electric field strength, E, in the ionization region. The profiles were modeled using the forward convolution method [27], accounting for the field strength, the finite time response of the apparatus (a Gaussian with 20 ns full-width-half-maximum) and the Doppler selection by the finite bandwidth of the probe laser (0.3 cm^{-1} at the one-photon wavenumber). Modeling of these profiles allowed extraction of the kinetic energy distributions (KEDs) and the anisotropy parameters.

Simultaneously with the action spectra, the room temperature vibrational absorption spectrum was monitored by PA spectroscopy. This was achieved by directing the residual of the NIR beam, after passing through the TOFMS, to a dichroic mirror which reflected it into an auxiliary PA cell. Wavelength calibration was accomplished by monitoring the rovibrational overtone spectra of water in this wavelength region and determining the wavelength according to the positions of the water absorption lines taken from the HITRAN database [31].

3. Results and discussion

Fig. 1 displays a representative PA spectrum and action spectra of ^{35}Cl, ^{35}Cl*, ^{37}Cl, and ^{37}Cl*
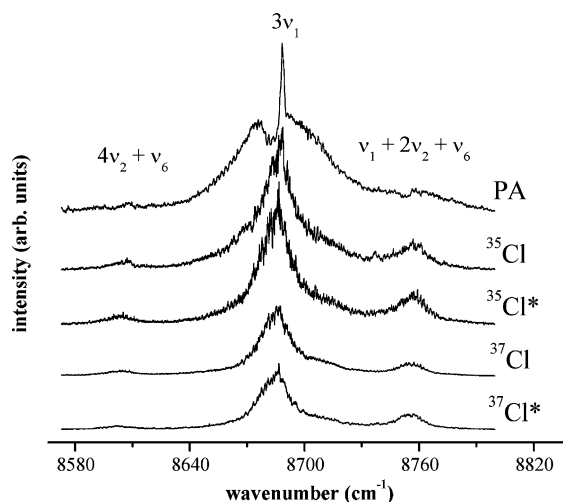

Fig. 1. Vibrational overtone spectra of CH_2Cl_2 in the region of second overtone of C–H stretch: room temperature photo-acoustic spectrum and jet-cooled action spectra of ^{35}Cl, ^{35}Cl*, ^{37}Cl, and ^{37}Cl*. The assignment of the bands is given above the spectra and relies on [32].

photofragments vs. the excitation laser wavelength in the region of the second C–H stretch overtone of CH_2Cl_2. Due to the occurrence of two stable Cl isotopes, the compound consists of an isotopic mixture of about 56% $CH_2{}^{35}Cl_2$, 38% $CH_2{}^{35}Cl^{37}Cl$, and 6% $CH_2{}^{37}Cl_2$. Therefore, the PA spectrum corresponds to contribution of all the isotopomers, whereas the ^{35}Cl or ^{35}Cl* action spectra are indicative of the first two isotopomers and the ^{37}Cl or ^{37}Cl* action of the last two. Comparison of the PA spectrum with the action spectra emphasizes the narrowing occurring in the latter due to reduction of the inhomogeneous structure. This is explicitly seen for the central A-type band where the P- and R-branches almost merge with the Q-branch in the action spectra, and also for the outer B-type bands which seem to be sharper in the action spectra than in the PA spectrum. Nonetheless, the general appearance of the features and the relative intensities of Cl and Cl* in the different bands of the action spectra seem to be comparable. This agrees with the behavior encountered in the VMP of CHF_2Cl and $CHFCl_2$ [23,24], but differs from that observed in VMP of CH_3Cl [14], where the action spectra of ^{35}Cl* and ^{37}Cl* were different. Moreover, the band

intensities in the PA and action spectra of CH_3Cl differed, and the $v_1 + 2v_4$ band was missing in the latter, implying dependence of the cross section for VMP on the initially excited vibrational state in the region of three quanta of C–H stretch.

Both the PA and action spectra of CH_2Cl_2 in the 8580–8800 cm^{-1} region comprise of several bands of different shapes. Relying on the results of Halonen [32], obtained with the curvilinear internal coordinate model, the bands at 8607, 8688, and 8755.7 cm^{-1} correspond to $4v_2 + v_6$, $3v_1$, and $v_1 + 2v_2 + v_6$, respectively. Accordingly, these bands are a result of the strong resonating levels of symmetric (v_1) and antisymmetric (v_6) C–H stretches and the stretching–HCH bending (v_2). The spectral splitting between the bands, Δv, is related to the recurrence period by $\tau = 1/c\Delta v$, allowing estimation of the intramolecular vibrational redistribution (IVR) time scale from half the period. In this manner, the redistribution time in CH_2Cl_2 pre-excited with three C–H quanta is estimated to be in the 0.20–0.25 ps range. These times are in between those encountered in molecules with an isolated C–H chromophore, $CHFCl_2$, CHF_2Cl, $CHCl_3$, and CHF_3 and in ethane derivatives, CH_3CF_2Cl and CH_3CFCl_2 excited to the second and third overtones [23]. This is since in the former the energy redistribution between C–H stretches and bends mostly takes less than 0.1 ps and in the extreme case less than 0.2 ps, while in the latter it is in the range of 0.25–0.65 ps. This behavior indicates that the mixing of stretches and bends via Fermi resonances leads to somewhat different redistribution times, where for molecules containing methylene groups it is somewhere in between those containing an isolated C–H group or a methyl group.

The ensuing action spectra are indicative of the increase in Cl and Cl* yield as a result of the photodissociation of vibrationally excited CH_2Cl_2 in the region of the second C–H stretch overtone. For that reason it is supposed that the enhanced reactivity in photodissociation of initially vibrationally excited molecules, relative to that of vibrationless ground state molecules, originates from the additional energy deposited into the vibrational states. Although this energy is deposited in the methylene C–H, it intramolecularly flows to

the C–Cl bond, which turns out to be the reaction coordinate, and results in more effective release of Cl atoms. It is evident that this energy flow occurs in less than a picosecond and is much faster than the time scale of the experiment, meaning that redistribution already occurred when the photodissociation takes place, as the pulse duration and the delay between excitation and dissociation are of the order of few nanoseconds. The photofragment yields mirror the vibrational excitation probability, measured by the PA spectrum, electronic transition moment, Franck–Condon (FC) overlap and the branching into the specific channel [22]. Therefore, it is likely that the vibrational excitation improves the FC factor of the vibrational modes containing C–Cl excitation and increases the combined energy (NIR + UV), leading to a better electronic transition and consequently to effective Cl loss.

The dynamics on the upper potential energy surfaces (PESs) may be assessed by the measurement of the branching into Cl and Cl* photoproducts and by the analysis of the measured TOF profiles. As mentioned above, the Cl*/Cl branching ratio was calculated from the Gaussian-fitted Doppler profiles, while considering the scaling factor of the REMPI transitions [30], and was found to be 0.55 ± 0.12. This ratio differs considerably from that found by Matsumi et al. [17], 0.25 ± 0.05 and by Tiemann et al. [7], 0.33 ± 0.03, in the 193 photodissociation of vibrationless ground state CH_2Cl_2. This is so, even if the Cl*/Cl ratio of Matsumi et al. [17], is corrected to 0.34 ± 0.07 after the new value of the two-photon oscillator strength ratio for the corresponding REMPI transitions is considered [33]. Since the combined energy used in the VMP of CH_2Cl_2, $\sim$51 180 cm^{-1}, is only slightly less than that used in the 193 nm photodissociation, 51 813 cm^{-1}, it seems unreasonable that the difference in energy led to the variation in the branching ratio. It should be noted that an increase in the branching into Cl* was also observed in the VMP of other chlorine containing molecules, including CH_3Cl, CHD_2Cl, CH_3CF_2Cl, and CH_3CFCl_2 [15,16, 23,24], but not in that of CHF_2Cl [26]. Therefore, the alteration of the branching ratio is probably due to the varied non-adiabatic dynamics in VMP,

which determines the fragment spin–orbit splitting during the departure from the molecule.

Support to this presumption comes also from the measured Cl and Cl* TOF profiles, displayed in Fig. 2a and taken with the polarization of the NIR laser perpendicular to the TOFMS axis and with that of the UV photolysis/probe laser parallel or perpendicular to the axis, respectively. Comparison of the profiles of Fig. 2a shows that their shapes differ considerably. The profile of ground state Cl is singly peaked for both polarizations and of the spin–orbit excited Cl* singly peaked for the perpendicular polarization and doubly peaked for the parallel one. This latter shape is ascribed to release of fragments with equal translational en-ergies but with velocities pointing toward and against the flight axis.

The spatial fragment distribution is represented by $P(v\theta) = P(v)[1 + \beta(v)P_2(\cos \theta)]$, where θ is the angle between the polarization direction of laser beam and the direction of the flight of the photofragments, $\beta(v)$ is the velocity-dependent anisotropy parameter, ranging from -1 for a perpendicular transition to $+2$ for a pure parallel transition, and P_2 is the second Legendre polynomial [34]. Evaluation of the β parameters and the center of mass (c.m.) translational energies of the Cl and Cl* photofragments was achieved via simulations of the TOF profiles by a forward convolution method, using a genetic algorithm that
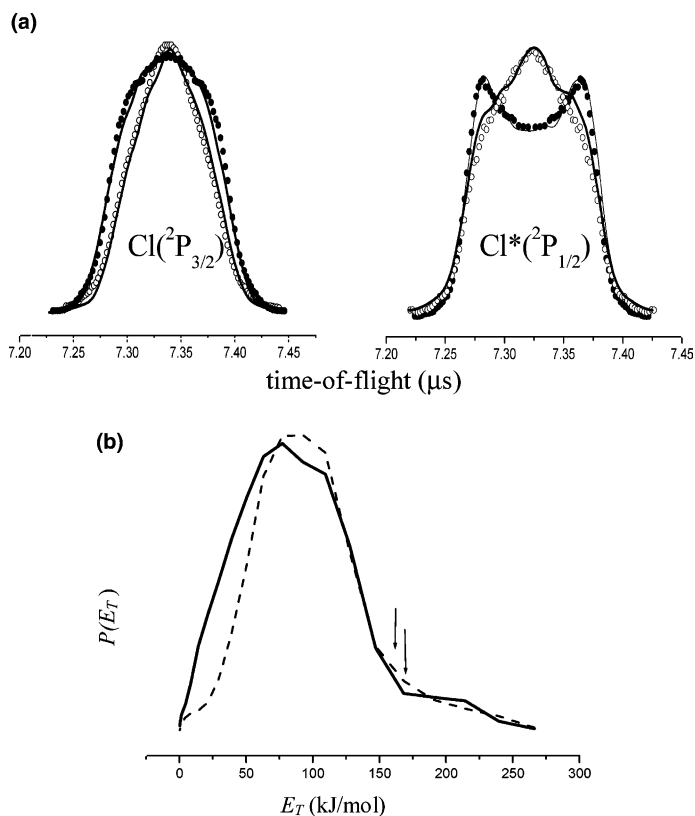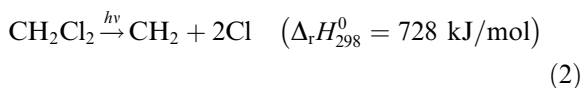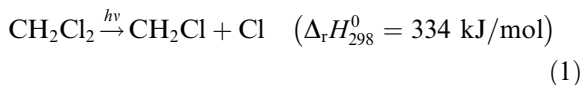

Fig. 2. Cl and Cl* photofragments produced in the ~235 nm photolysis of CH_2Cl_2 pre-excited to the Q-branch of $3v_1$ (a) arrival time profiles, where open circles and solid points are the experimental data points taken with the polarization of the UV photolysis/probe laser parallel and perpendicular, respectively, to the TOFMS axis. The polarization of the overtone excitation laser was perpendicular to the TOFMS axis. Solid lines are the simulations of the corresponding profiles, denoting the best fit energy distributions, (b) energy distributions of Cl (solid line) and Cl* (dashed line), extracted from the corresponding arrival profiles. The arrows indicate the maximum possible energies calculated for release of one chlorine atom.

minimized the deviation of the simulated profile from the measured one [27]. Single velocity-independent and identical β parameters were used to simultaneously fit the profiles obtained in both polarization geometries. Even so, the measured arrival profiles (solid points and open circles) were well fitted by the simulations represented by solid lines (Fig. 2a) resulting in the optimized translational energy distributions shown in Fig. 2b. These distributions are fairly broad, centering at relatively high energies.

Some insight regarding the maximum translational energy that should be channeled in the released Cl and Cl* photofragments can be obtained from consideration of the energetics of the potential dissociation channels. The combined energy used for excitation of the CH_2Cl_2 molecules from the vibrationless ground state to the second C–H stretch overtone and subsequently to the A-band is $\sim 51\,180$ cm^{-1} (612 kJ/mol). The energy required for chlorine atoms release was calculated from the standard enthalpies of formation ($\Delta_f H^0$) of the involved molecule and radicals [35]

$$CH_2Cl_2 \xrightarrow{h\nu} CH_2Cl + Cl \quad (\Delta_r H^0_{298} = 334 \text{ kJ/mol}) \tag{1}$$

$$CH_2Cl_2 \xrightarrow{h\nu} CH_2 + 2Cl \quad (\Delta_r H^0_{298} = 728 \text{ kJ/mol}) \tag{2}$$

The reaction enthalpy, $\Delta_r H^0_{298}$, for the release of Cl* atoms via channels (1) and (2) should be 10.6 and 21.2 kJ/mol higher. It is obvious that the combined energy is not enough for the release of two ground state chlorine atoms but exceeds that required for the loss of one atom, implying that the maximum translational energy released via (1) should be 162 and 156 kJ/mol for Cl and Cl*, respectively. These energies are marked by the arrows in the KEDs of Fig. 2b and should be somewhat higher providing that $\Delta_r H^0_0$ were retrieved. Anyhow, as seen from the energy distribution, these maximal energies are reached in the dissociation of CH_2Cl_2 and since the distributions are broad and centered at large energies it seems reasonable that direct dissociation took place on repulsive potential energy surfaces.

Further information regarding the bond breaking mechanism can be gained from the determined β parameters. This is since the magnitude and sign of β provide information regarding the orientation of the transition dipole moment μ in the parent molecule, the symmetry of the involved excited state(s) and the excited state lifetime. The β parameters evaluated from our experimental data were 0.14 ± 0.04 for Cl and 0.37 ± 0.05 for Cl*, with errors calculated from the scattering of the 10 'best' β parameters obtained from the above-mentioned simulations. Actually, the CH_2Cl_2 is of C_{2v} symmetry, however, because of the C–H vibrational excitation the geometry of the molecule is distorted and therefore its C_s dissociation should be considered. It is believed that transitions from the vibrationally excited state of the A$'$ ground state may access repulsive states of either A$'$ or A$''$ symmetry. For CH_2Cl_2, the observed positive β value suggests that μ is parallel to the line linking the two chlorine atoms and perpendicular to the CH_2 plane, corresponding to an A$'' \leftarrow$ A$'$ electronic transition. Accounting for the initial upper state geometry, with a Cl–C–Cl bond angle of 112°, the theoretical limit of β for this transition should be ~ 1.1. Even though the observed β parameters for ejection of Cl and Cl* photofragments were positive, they were considerably smaller than the estimated limiting values reflecting a partial loss of anisotropy. This loss could arise either from rotational motion during slow dissociation or from some dynamical factor. The former is unlikely due to the accessibility of the upper dissociative states, the promptness of the dissociation and the large release of fragment translational energy. It is rather some contribution of an electronic transition of A$' \leftarrow$ A$'$, which reaches a β value of -1 in the limit of prompt dissociation that could reduce the β parameters. Therefore, the positive measured β parameters of both photofragments might point toward production of both Cl and Cl* as a result of simultaneous absorption to both A$'$ and A$''$ states and non-adiabatic curve crossing. Since the β parameter of Cl* is larger than that of Cl, it is anticipated that the contribution of the A$''$ state to the former channel is more effective. Absorption via more than one PES and curve crossings were suggested to account for

the observed branching ratios and the anisotropies in other halocarbons as well, exemplified by CH_3I [2], CH_3Cl and CHD_2Cl [15,16], $CHFCl_2$ [24,25], CH_3CFCl_2 [28], CH_2BrCl [18], CF_2Br_2 [19], and CH_2I_2 [20].

4. Conclusions

The intramolecular dynamics of dichloromethane was studied via ∼235 nm photodissociation of vibrationally excited molecules with three C–H quanta. The vibrational overtone spectra consist of bands related to C–H stretches and to combination of stretching and HCH bending, implying sub-picosecond energy redistribution. Evidence to energy flow, out of the initially excited C–H stretch into the C–Cl reaction coordinate, comes also from the enhanced production of Cl and Cl* photoproducts. The dissociation is rapid, resulting dominantly in chlorine elimination with preferred formation of ground state over spin–orbit excited Cl. The observed Cl*/Cl branching ratio in the VMP experiment is higher than that obtained in the direct, almost isoenergetic, 193 nm photodissociation of CH_2Cl_2 suggesting that the dynamics proceeds more non-adiabatically in the former. The non-adiabaticity of the process is also supported by the measured anisotropy parameters. Their values are lower than the limiting values of ∼1.1 for a pure $A'' \leftarrow A'$ transition indicating that A' states are also involved, resulting in mixing via curve crossing and releasing Cl and Cl*. Further experiments that will initially excite higher C–H overtones and then will be promoted to the upper PESs are necessary to assess their effect on branching ratios and anisotropy parameters.

Acknowledgements

References

[1] M. Shapiro, J. Phys. Chem. 90 (1986) 3644.
[2] S. Yabushita, K. Morokuma, Chem. Phys. Lett. 153 (1988) 517.
[3] Y. Amatatsu, K. Morokuma, S. Yabushita, J. Chem. Phys. 94 (1991) 4858.
[4] H. Guo, J. Chem. Phys. 96 (1992) 2731.
[5] D. Xie, H. Guo, Y. Amatatsu, R. Kosloff, J. Phys. Chem. A 104 (2000) 1009.
[6] S.J. Riley, K.R. Wilson, Faraday Discuss. Chem. Soc. 53 (1972) 132.
[7] E. Tiemann, H. Kanamori, E. Hirota, J. Chem. Phys. 88 (1988) 2457.
[8] R.E. Continetti, B.A. Balko, Y.T. Lee, J. Chem. Phys. 89 (1988) 3383.
[9] R.O. Loo, H.-P. Haerri, G.E. Hall, P.L. Houston, J. Chem. Phys. 90 (1989) 4222.
[10] A.T.J.B. Eppink, D.H. Parker, J. Chem. Phys. 110 (1999) 832.
[11] A.J. van den Brom, M.L. Lipciuc, M.H.M. Janssen, Chem. Phys. Lett. 368 (2003) 324.
[12] J.G. Underwood, I. Powis, Phys. Chem. Chem. Phys. 2 (2000) 747.
[13] W.P. Hess, D.W. Chandler, J.W. Thoman, Chem. Phys. 163 (1992) 277.
[14] C. Tao, P.J. Dagdigian, Chem. Phys. Lett. 350 (2001) 63.
[15] H.M. Lambert, P.J. Dagdigian, Chem. Phys. Lett. 275 (1997) 499.
[16] H.M. Lambert, P.J. Dagdigian, J. Chem. Phys. 109 (1998) 7810.
[17] Y. Matsumi, K. Tonokura, M. Kawasaki, G. Inoue, S. Satyapal, R. Bersohn, J. Chem. Phys. 97 (1992) 5261.
[18] P. Zou, W.S. McGivern, S.W. North, Phys. Chem. Chem. Phys. 2 (2000) 3785.
[19] M.S. Park, T.K. Kim, S.H. Lee, K.H. Jung, H.R. Volpp, J. Wolfrum, J. Phys. Chem. A 105 (2001) 5606.
[20] H. Xu, Y. Guo, S. Liu, X. Ma, D. Dai, G. Sha, J. Chem. Phys. 117 (2002) 5722.
[21] F.F. Crim, J. Phys. Chem. 100 (1996) 12725.
[22] I. Bar, S. Rosenwaks, Int. Rev. Phys. Chem. 20 (2001) 711.
[23] G. Dorfman, A. Melchior, S. Rosenwaks, I. Bar, J. Phys. Chem. A 106 (2002) 8285.
[24] A. Melchior, X. Chen, I. Bar, S. Rosenwaks, J. Chem. Phys. 112 (2000) 10787.
[25] A. Melchior, I. Bar, S. Rosenwaks, J. Chem. Phys. 107 (1997) 8476.
[26] L. Li, G. Dorfman, A. Melchior, S. Rosenwaks, I. Bar, J. Chem. Phys. 116 (2002) 1869.
[27] X. Chen, R. Marom, S. Rosenwaks, I. Bar, T. Einfeld, C. Maul, K.H. Gericke, J. Chem. Phys. 114 (2001) 9033.

[28] T. Einfeld, C. Maul, K.H. Gericke, R. Marom, S. Rosenwaks, I. Bar, J. Chem. Phys. 115 (2001) 6401.

[29] C. Hubrich, F. Stuhl, J. Photochem. 12 (1980) 93.

[30] P.M. Regan, S.R. Langford, D. Ascenzi, P.A. Cook, A.J. Orr-Ewing, M.N.R. Ashfold, Phys. Chem. Chem. Phys. 1 (1999) 3247.

[31] L.S. Rothman, C.P.Rinsland, A. Goldman, S.T. Massie, D.P. Edwards, J.-M. Flaud, A. Perrin, C. Camy-Peyret, V. Dana, J.-Y. Mandin, J. Schroeder, A. McCann, R.R. Gamache, R.B. Wattson, K.Yoshino, K. Chance, K. Jucks, L.R. Brown, V. Nemtchinov, P.Varanasi, The 1996 HITRAN Molecular Spectroscopic Database and HAWKS (HITRAN Atmospheric Workstation).

[32] L. Halonen, J. Chem. Phys. 88 (1988) 7599.

[33] J. Zhang, M. Dulligan, C. Wittig, J. Chem. Phys. 107 (1997) 1403.

[34] R.N. Zare, Mol. Photochem. 4 (1972) 1.

[35] R. Atkinson, D.L. Baulch, R.A. Cox, R.F. Hampson Jr., J.A. Kerr, M.J. Rossi, J. Troe, J. Phys. Chem. Ref. Data 29 (2000) 167.